

On-Chip Universal Linear Optics using a 4x4 Silicon Photonic Coherent Crossbar

George Giamougiannis⁽¹⁾, Miltiadis Moralis-Pegios⁽¹⁾, Apostolos Tsakyridis⁽¹⁾, Nikos Bamiedakis⁽²⁾, David Lazovsky⁽²⁾, Nikos Pleros⁽¹⁾

⁽¹⁾Department of Informatics, Center for Interdisciplinary Research & Innovation, Aristotle University of Thessaloniki, Thessaloniki, Greece

⁽²⁾Celestial AI, 100 Mathilda Place, Suite 170, Campbell, CA 95008, United States
e-mail address: giamouge@csd.auth.gr

Abstract: We demonstrate the first on-chip and fidelity-restorable universal linear optical circuit that relies on a novel 4×4 silicon photonic coherent crossbar architecture. Its experimental characterization yields a fidelity of 99.93±0.06%, calculated over 10,000 arbitrary matrices.

1. Introduction

The recent resurgence of interest in linear optical circuits is engendering novel applications in the fields of quantum and optical information processing. With the ultimate target being the realization of linear transformations between optical modes, several experimental demonstrations have been proposed so far, mainly relying on coherent interferometric layouts that perform unitary transformations [1-2]. This leads to arbitrary matrix implementations by exploiting the singular value decomposition (SVD) technique and two cascaded unitary layouts [3-4]. Due to the increased complexity required for designing and fabricating SVD-based optical architectures [5], all coherent on-chip experimental demonstrations have been unitary circuit implementations [1-2], with universal linear transformations presented only via the reuse of the same on-chip unitary circuit [5]. On top of that, the dominant unitary linear optical circuit architectures rely on the U(2) algebraic decomposition framework that requires cascaded 2×2 Mach-Zehnder interferometers (MZIs) either in a triangular [6] or rectangular [7] mesh configuration. This inevitably leads to i) differential path losses that significantly degrade the fidelity performance as the circuit size or the node loss increase, ii) the absence of any fidelity-restoration mechanism that could be employed, without embedding extra in-circuit monitors, iii) the need for ultra-low loss MZI nodes, restricting in this way the transformation-speed credentials of the input optical modes and, finally, iv) the need for recursive programming algorithms with an O(N) complexity scaling.

We have recently proposed a novel coherent photonic crossbar (Xbar) architecture [8] that migrates from existing U(2)- or SVD-based layouts and can realize arbitrary linear transformations, overcoming all disadvantages of state-of-the-art SVD-based schemes while supporting simple single-step programming of O(1) complexity. In this paper, we experimentally demonstrate, for the first time, an on-chip universal linear optical circuit using a silicon photonic (SiPho) coherent linear operator that performs arbitrary transformations with a fidelity of 99.93±0.06%. It relies on the recently formulated photonic Xbar architecture [8] and comprises a coherent 4×4 SiPho Xbar that utilizes SiGe electro-absorption modulators (EAMs) and thermo-optic (TO) phase shifters (PSs) for executing the transformations between the optical modes, with its experimentally measured insertion losses (IL) closely matching the theoretical predictions of [8]. A maximum IL discrepancy of 1.42 dB was measured between the Xbar output ports, which can be balanced through external attenuators, allowing for fidelity restoration. Experimental evaluation of the fidelity-restored photonic Xbar over a number of 24 permutation matrices and 10,000 arbitrary real-matrix implementations revealed a record-high average transformation fidelity of 99.93% in both cases.

2. Coherent photonic Crossbar: Architecture, 4×4 prototype & experimental setup

The architecture of the proposed N×N coherent Xbar is illustrated in Fig. 1(a) and follows the layout presented in [8]. An N-elements long input vector is hardware encoded to an array of modulators, highlighted in the red rectangle of Fig. 1(a), that are employed at the output of an 1:N splitting stage. The input vector is then broadcasted into the N columns of the optical matrix via directional couplers (DCs). The N×N transformation matrix elements are directly mapped onto the N² Xbar nodes highlighted in the blue rectangle of Fig. 1(a). Every Xbar node involves an intensity modulator for imprinting the absolute value of the corresponding matrix element, while its sign is encoded in the phase of the electric field via a phase shifting element [8]. The weighted elements of the input vector are recombined via an N:1 coupling stage at every Xbar column output, realizing the targeted linear transformation. Finally, a bias branch can be employed for enabling the sign information of the output electric fields of every column, following the principle described in [9]. The proposed architecture can be loss-balanced by-design by compensating for any inter-column differential losses through the use of different coupling ratios in the DCs employed in every column [8]. However, even in the case of different losses experienced at every Xbar column, an array of attenuating elements can be deployed at every Xbar column output to equalize inter-column losses and ameliorate the fidelity of the linear transformations.

Figure 1(b) illustrates a microscope photo of the fabricated 4×4 coherent Xbar processor and the experimental setup established for its evaluation. The photonic chip was fabricated in imec's ISSIPP50G platform using pdk-ready components and incorporates 50 um-long, 50 GHz SiGe EAMs [10] as input vector and matrix node intensity modulators, while TO PSs were utilized for the sign imprinting at every matrix node. Light from a tunable laser source was injected through a TE grating coupler to the input of the photonic processor, while a multi-channel power meter (PM) was employed to measure the optical power emerging at each of its output ports. It is worth noted that column 4 experienced unexpectedly high losses that were probably owed to damaged I/O coupling. A multi-channel digital-to-analog converter (DAC) was used to fine tune the TO PSs and encode the targeted transformation matrix elements onto the Xbar nodes according to a look-up-table that correlates the matrix values to the EAM driving voltages.

Figure 1(c) depicts the experimentally measured IL and extinction ratio (ER) values of a single stand-alone 50um-long EAM across the C-band, for different values of the EAM reverse bias voltage between 0 to 3V in steps of 0.5V. Fig. 1(d) illustrates the spectral response recorded at the output of the 2nd Xbar column when all input vector EAMs were driven at 0V and all intra-column EAMs are biased at either 0V (blue curve) or 3V (orange curve), with similar curves obtained also at column outputs 1 and 3. A resonant behavior can be observed that can be avoided in future fabrication runs by synchronizing the optical path lengths within the 4-branch multiport interferometer formed between the Xbar input and the column output. Fitting the acquired transfer function envelope data to 2nd order polynomials, we calculate the imposed IL and achieved ER across the 1540-1580 nm band. These metrics are plotted in Fig. 1(e) together with a figure-of-merit (FOM) that correlates ER and IL at the column output and is expressed as $FOM = ER(dB)/IL(dB)$. A maximum FOM of ~0,26 is obtained at $\lambda = 1563\text{ nm}$, providing the optimum operational wavelength. Finally, Fig. 1(f) puts in juxtaposition the theoretically expected IL curve for different matrix dimensions together with the experimentally derived optical losses for the 4×4 matrix layout and its previously demonstrated 2×1 precursor [11] (extrapolated into a 2×2 design). The experimental Xbar IL values were obtained on a per column basis taking into account the IL of both the input vector and the matrix stages, normalized over the I/O coupling losses. All input and node EAMs were driven at 0V, so as to represent an input vector of [1,1,1,1] and an all-ones matrix. The theoretical curve follows the mathematical framework analyzed in [8], with the loss parameters for the different building blocks based on the respective experimental values. As can be observed, the theoretical and experimental scatter points closely match with a deviation within a range of (0.6, 2) dB.

3. Experimental Results

To verify the reconfigurability and showcase the inter-column fidelity restoration mechanism of the Xbar photonic processor, an input vector of [1, 1, 1, 1] was enforced by driving the input EAMs at 0V and an initial number of 256 4×3 targeted arbitrary transformation matrices $T[i]$ was realized on-chip. The electrical field intensities Y_i obtained at

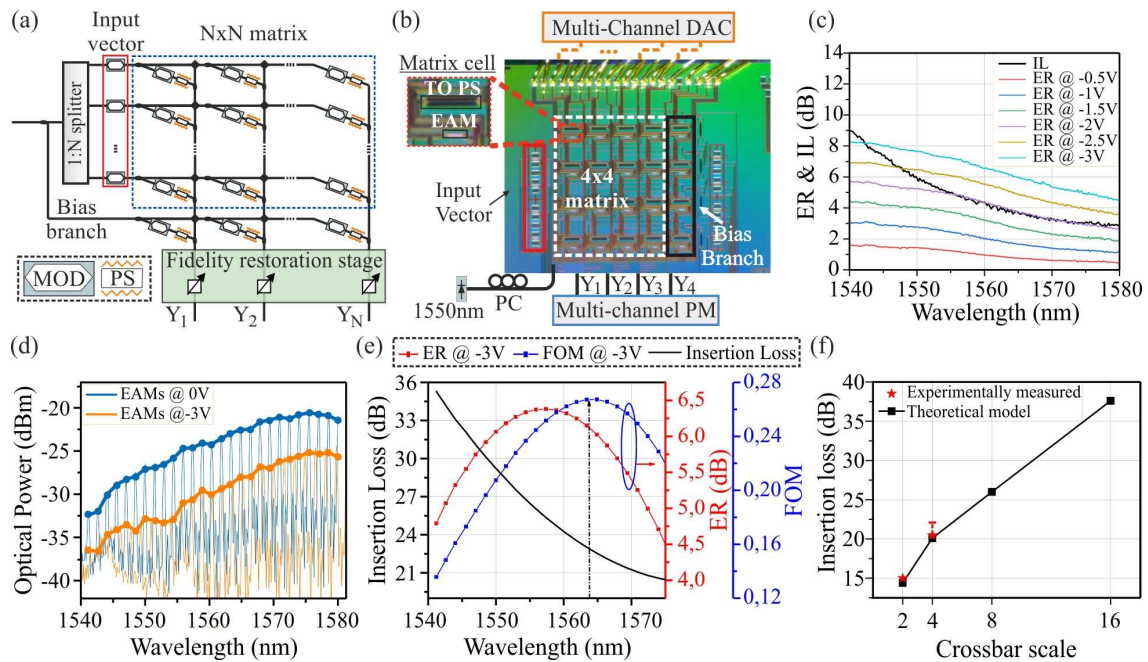


Fig. 1. (a) N×N Xbar architecture. (b) Microscope photo and experimental setup of the 4×4 Xbar prototype. (c) Standalone 50 um SiGe EAM characterization (d) Optical spectrum of 4×4 Xbar's column 2 when constituent EAMs are driven at 0 and -3V. (e) Fitted IL, ER and FOM of column 2. (f) Comparison of theoretical projections versus experimental measurements.

each i -th ($i \in \{1,2,3\}$) Xbar column were then measured, providing this way the matrix-vector multiplication $Y_i = [1, 1, 1, 1] * T$. The target matrix elements $T_{i,j}$ were considered to be real positive values with $T_{i,j} \in \{0, 0.18, 0.46, 1\}$, with their respective experimentally enforced values provided by 4 different EAM driving voltages of $V_{EAM} \in \{-3, -2, -1, -0\}V$. Interferometer calibration and coherent addition at every Xbar output was achieved by fine tuning the TO PSs within the Xbar nodes via an automated optimization algorithm. Figure 2(a) illustrates the distribution of the optical powers emerging at the three functional Xbar column outputs when all 256 target matrices are experimentally encoded, showing that the per column optical output power levels range within ~ 7 dB. The inter-column differential loss can be quantified by fitting the histogram data at every column to a gaussian distribution and comparing their mean values, with their maximum difference equalling ~ 1.42 dB. This calibration process allows us to compensate the differential inter-column losses via respective attenuation factors realized in the fidelity restoration stage of the Xbar architecture, leading in this way to a perfectly inter-column loss-balanced layout [8].

The performance of the fidelity-restored photonic processor was then assessed by implementing experimentally 10,024 (all 24 possible permutation and 10,000 arbitrary) different matrices. Fig. 2(b) illustrates the implementation of an indicative permutation matrix with the bar chart showing the normalized power levels obtained at the three column outputs. The maximum inter-column deviation is only 2.2%. Figure 2(c) depicts the Xbar configuration when implementing an arbitrary matrix with all its first column elements being one and all its four values within the 2nd and 3rd matrix columns equalling zero. The bar chart indicates the experimentally obtained $[1,0,0]$ output vector, with the residual optical power in the Xbar output columns 2&3 corresponding to the finite ER of the associated EAM cells. Finally, the average accuracy over the entire set of 10,024 arbitrary matrix implementations was quantified via the fidelity metric that is based on the Frobenius inner product of the targeted (Y_{targ}) and the experimentally obtained (Y_{exp}) output vectors, when considering an all-one input vector, given by the expression $F(Y_{exp}, Y_{targ}) = \left| \frac{\text{tr}(Y_{targ}^T Y_{exp})}{\sqrt{\text{tr}(Y_{targ}^T Y_{targ}) \text{tr}(Y_{exp}^T Y_{exp})}} \right|^2$. Figure 2(d) illustrates the obtained results, revealing that all arbitrary matrix implementations had a fidelity higher than 99.55%, with their fidelity value being as high as $99.93 \pm 0.07\%$.

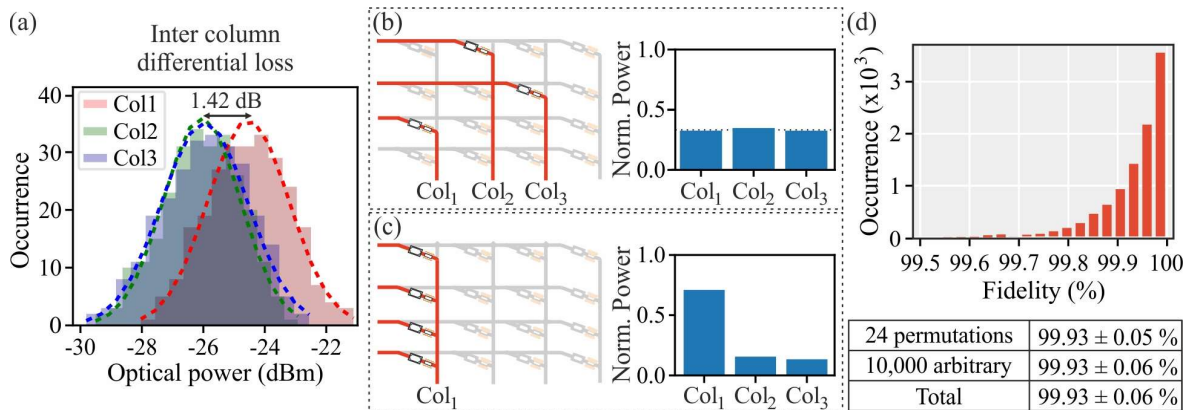


Fig. 2. (a) Histograms of optical powers emerging at Column 1-3, when implementing 256 identical transformation matrices. (b),(c) Schematic representation of two indicative transformation matrices with the resulting normalized output power intensities. (d) Calculated fidelity performance during the implementation of 10,024 permutation and arbitrary transformation matrices.

4. Acknowledgements

This work was supported by the EC through H2020 project SiPHO-G (779664) and by the GSRT through project DeepLight (4233).

5. References

- [1] A. Ribeiro et al., "Demonstration of a 4×4 -port universal linear circuit", *Optica* 3, 1348-1357 (2016)
- [2] C. Taballione et al., "20-Mode Universal Quantum Photonic Processor", arXiv:2203.01801.
- [3] D. A. B. Miller, "Self-configuring universal linear optical component" [Invited], *Photon. Res.* 1, 1-15 (2013).
- [4] Y. Shen, et al., "Deep learning with coherent nanophotonic circuits", *Nature Photon* 11, 441-446 (2017).
- [5] D. A. B. Miller, "How complicated must an optical component be?", *J. Opt. Soc. Am. A* 30, 238-251 (2013).
- [6] M. Reck, et al., "Experimental realization of any discrete unitary operator", *Phys. Rev. Lett.* 73, 58-61 (1994).
- [7] W. R. Clements, et al., "Optimal design for universal multiport interferometers", *Optica* 3, 1460-1465 (2016).
- [8] G. Giamougiannis et al., "Coherent photonic crossbar as a universal linear operator", arXiv:2208.12033.
- [9] G. Mourgiyas-Alexandris et al., "Neuromorphic Photonics With Coherent Linear Neurons Using Dual-IQ Modulation Cells" in JLT 2020.
- [10] M. Pantouvaki et al., "Active Components for 50 Gb/s NRZ-OOK Optical Interconnects in a Silicon Photonics Platform" in JLT 2017
- [11] G. Giamougiannis et al., "Silicon-integrated coherent neurons with 32GMAC/sec/axon compute line-rates using EAM-based input and weighting cells", ECOC 2021